PROFESSOR LINGXIA LI (Orcid ID : 0000-0003-2860-9312)

DR SHIHUI YU (Orcid ID : 0000-0003-2829-4533)

Article type : Rapid Communication

High dielectric constant and high–Q in microwave ceramics of $SrTiO_3$ co–doped with aluminum and niobium

Siliang Chen, Lingxia Li[†], Shihui Yu[†], Haoran Zheng, Zheng Sun

School of Microelectronics and Key Laboratory for Advanced Ceramics and Machining Technology of Ministry of Education; Tianjin 300072, China

[†] Corresponding author. Tel./fax: +86 2227402838.

E-mail: lingxia66@163.com (L. Li)

[†] Corresponding author. Tel./fax: +86 2227402838.

E-mail: ysh728@126.com (S. Yu)

This article has been accepted for publication and undergone full peer review but has not been through the copyediting, typesetting, pagination and proofreading process, which may lead to differences between this version and the Version of Record. Please cite this article as doi: 10.1111/jace.15413

Abstract

Al/Nb co–doped $SrTiO_3$ microwave ceramics with the composition of $SrTi_{1-x}(Al_{0.5}Nb_{0.5})_xO_3$ (x = 0.03, 0.05, 0.1 and 0.15) have been synthesized via a standard solid–state reaction method. The substitution of $(Al_{0.5}Nb_{0.5})^{4+}$ in B–site inhibits the reduction of Ti^{4+} ions and the growth of grain size, then the transport of mobile charge carriers is limited, and thus the Q value is improved. For the $SrTi_{0.9}(Al_{0.5}Nb_{0.5})_{0.1}O_3$ ceramics, in addition to their high dielectric constant (ε_r ~185), they exhibit correspondingly a high Qf value (~ 9077 GHz) at 2.9 GHz, making the microwave ceramics suitable for myriad device miniaturization and high performance wireless communication.

KEYWORDS: dielectric materials/properties; electroceramics; microwaves

1 INTRODUCTION

In the past few decades, the proliferation of commercial wireless technologies has brought increasing demands on the performance of high–frequency equipments and applications applying in the microwave range.[1–3] To further minimize the size of microwave devices, it is urgent to increase the dielectric constant (ε_r) and reduce the dielectric loss of microwave dielectric materials.[4–5] Therefore, the dielectric materials with high ε_r and quality factors (Qf) have been given much attention. Recently, high dielectric constant $SrTiO_3$ ceramics have been explored,[6–7] however, the relatively low Qf (~3000) severely limits their practical application. Related studies show that oxygen loss occurs in most titanate–based materials under high sintering temperature, resulting in partially reduction of Ti^{4+} to Ti^{3+} and increase of dielectric loss.[8–10] Some researchers found that substitution of acceptor and donor ions combination at Ti–site can improve the microstructure and restrain the reduction of Ti^{4+} in titanate–based materials, and thus enhances the dielectric properties.[11–12]

In this study, Al^{3+} as an acceptor and Nb^{5+} as a donor substituting for Ti^{4+} in B site were co-doped in $SrTiO_3$ based ceramics to reduce the dielectric loss. The substitution of combinations of aliovalent cations $(Al_{0.5}Nb_{0.5})^{4+}$ keeps the charge balance and structural stability. The influences of the isovalent substitution of $(Al_{0.5}Nb_{0.5})^{4+}$ on microstructure and microwave dielectric properties of $SrTiO_3$ are discussed, and the influence of grain boundaries on properties of materials are studied comparatively.

2 EXPERIMENTAL PROCEDURE

$SrTi_{1-x}(Al_{0.5}Nb_{0.5})_xO_3$ (x = 0.03, 0.05, 0.1 and 0.15) ceramics were prepared by a conventional solid state reaction method from high–purity powders of $SrCO_3$ (99.9%), Al_2O_3(99.9%), Nb_2O_5 (99.99%) and TiO_2 (99.9%).The starting powders were mixed and grounded with ZrO_2 balls in ethanol for 6 h. Then, the powders were dried and calcined at 1150 °C for 4 h, and pressed into pellets. The pellets were sintered at 1350

°C for 4 h in air. After the sintering temperature has dropped to 800 °C at a rate of 1 °C/min, the sintered pellets were furnace cooled to room temperature.

The crystal structure was examined by Powder X–ray diffraction analysis (D/MAX–2500; Rigaku, Tokyo, Japan) using Cu–K_α radiation. The microstructure was observed by field emission scanning electron microscopy (FE–SEM, S–4800; Hitachi, Ltd., Tokyo, Japan). Microwave dielectric properties were carried out by a network analyzer (8720ES; Agilent, Santa Clara, CA) in the frequency range of 2–4.5 GHz. The dielectric constant (ε_r) and quality factor (Qf) values were measured by Hakki–Coleman's method using TE_{011} resonant modes,[5] and the temperature coefficient of resonant frequency (τ_f) values were evaluated by the resonant–cavity method.[13] The leakage current was analyzed by a high resistance meter (Agilent4339B, Santa Clara, CA) at room temperature.

3 RESULTS AND DISCUSSION

The XRD patterns of $SrTi_{1-x}(Al_{0.5}Nb_{0.5})_xO_3$ ($0 \le x \le 0.15$) ceramics are illustrated in Fig. 1(a). A perovskite structure is identified in all components. The diffraction peaks are indexed according to the standard pattern of $SrTiO_3$ (JCPDS #86–0179). The tolerance factors (t) of $SrTi_{1-x}(Al_{0.5}Nb_{0.5})_xO_3$ ceramics are calculated by the following equation:[14–15]

$$t = \frac{r_A + r_O}{\sqrt{2} \times \left(\frac{r_{B'} + r_{B''}}{2} + r_O\right)} \quad (1)$$

where r_A, r_O, $r_{B'}$, and $r_{B''}$ are the crystal radius of the Sr^{3+}, Ti^{4+}, $(Al_{0.5}Nb_{0.5})^{4+}$ and O^{2+} ions, respectively. With x value increases from 0 to 0.15, the tolerance factor of $SrTiO_3$ slightly increases from 0.9987 to 1.008, which indicates a stable perovskite structure for all the compositions. According to previous studies by Glazer[16] and Reaney[17], the entire process has no octahedral tilting thus it has no influence on the change of crystalline phase. With the increase of doping content, the diffraction peaks displace to higher 2θ angles, which reflects that the reduction of unit cell volume due to the substitution of Ti^{4+} (0.605 Å) by $(Al_{0.5}Nb_{0.5})^{4+}$ (0.586 Å) in B site. Fig. 1(b) indicates the (200) peak around the 2θ of 46.4°. The appearance of asymmetry and splitting in XRD patterns with doping content increases may be attributed to the pseudo cubic and/or tetragonal distortion.[18]

The SEM images from the as–sintered surface of $SrTi_{1-x}(Al_{0.5}Nb_{0.5})_xO_3$ ($0 \le x \le 0.15$) ceramics are shown in Fig. 2. Ceramics with dense microstructure are prepared in each component. As shown in Fig. 2 (a), the average grain size of pure $SrTiO_3$ is extremely large (~50 μm). After addition of Al^{3+} and Nb^{5+}, the average grain size decreases dramatically to ~7.29 μm for the $SrTi_{0.05}(Al_{0.5}Nb_{0.5})_{0.95}O_3$ (As shown in Fig. 2 (b)). As some ions tend to segregate at the grain boundaries, the growth of grain is restrained.[19] As a result, the grains tend to become small and uniform with the increment of doping content. As presented in Fig. 2 (c) and (d), the average grain size decreases to ~1.30 μm when x = 0.1 and becomes a little smaller at x = 0.15. It is worth noting that the morphology of grain is greatly changed when x ≥ 0.1, which may be due to the pseudo cubic and/or tetragonal distortion. The decrease of average grain size would lead to an increase in the grain boundary number, resulting in the aggregation of defects and impurities.[20] As the SEM images show, pores begin to appear when x = 0.15, which increases the porosity obviously.

The dielectric constants of $SrTi_{1-x}(Al_{0.5}Nb_{0.5})_xO_3$ ($0 \leq x \leq 0.15$) ceramics are shown in Fig. 3. The dielectric constant decreases approximately linearly as x value increases from x = 0 to 0.15. The dielectric constant of the pure $SrTiO_3$ ceramics is 305, which is similar to those reported in the literature,[21] and the dielectric constant drops to 146 when the x reaches 0.15. According to the Shannon additive rule,[22] the theoretical dielectric polarizability (a_{the}) can be calculated as follow:

$$\alpha_{the}[SrTi_{1-x}(Al_{0.5}Nb_{0.5})_xO_3]$$

$$= \alpha(Sr^{2+}) + (1-x)\alpha(Ti^{4+}) + 0.5x\alpha(Al^{3+}) + 0.5x\alpha(Nb^{5+}) + 3(O^{2-}) \qquad (2)$$

where αi (i: Sr^{2+}, Ti^{4+}, Al^{3+}, Nb^{5+}, O^{2-}) is the dielectric polarizability of corresponding ions. The calculated values are shown in Fig. 3. The dielectric constant would continually fall as the amount of dopant increases because of the smaller polarizability of $(Al_{0.5}Nb_{0.5})^{4+}$ (2.38 $Å^3$) than Ti^{4+} (2.93 $Å^3$).[23]

The Qf values of $SrTi_{1-x}(Al_{0.5}Nb_{0.5})_xO_3$ ($0 \leq x \leq 0.15$) ceramics are exhibited in Fig. 4(a). The Qf value increases from 3072 GHz to 9077 GHz when x increases from 0 to 0.1, then falls to 7038 GHz when x = 0.15. For titanate dielectric materials, the reduction of Ti^{4+} is the main factor affecting the decrease of Qf value, the procedure is shown as follows:[6]

$$O_O^{\times} \leftrightarrow V_O^{\cdot\cdot} + 2e' + \frac{1}{2}O_2 \quad (3)$$

$$Ti_{Ti}^{\times} + e' \leftrightarrow Ti_{Ti}' \quad (4)$$

Isovalent Al/Nb co-substitution for Ti could suppress the process effectively. The Nb^{5+} ions enter B site of $SrTiO_3$ as doping donors, and the donors are electronically compensated as the following reaction:[24]

$$2SrO + Nb_2O_5 \rightarrow 2Sr_{Sr} + 2Nb_{Ti}^{\cdot} + 6O_O + \frac{1}{2}O_2 + 2e' \quad (5)$$

While Al^{3+} ions are doped as acceptors and compensated by oxygen vacancies via:

$$2SrO + Al_2O_3 \rightarrow 2Sr_{Sr} + 2Al_{Ti}' + 5O_O + V_O^{\cdot\cdot} \quad (6)$$

According to Eq. (6) and Eq. (3), the generation of oxygen vacancies reduces the number of electrons effectively. Meanwhile, a small amount of donor doping in Eq. (5) would react with oxygen vacancies thus lessening the defects instead of reducing Ti^{4+} ions. In addition to the suppressing of Ti^{4+} reduction, the Qf values are also improved by the annealing process, presumably resulting in the re-oxidation behavior.[25] The significantly decreased grain size makes re-oxidation even easier to penetrate the fine grains, and subsequently contribute to the reduced dielectric loss and improved Qf values.

The influence of carriers on dielectric loss can be demonstrated by leakage current test. The leakage current of $SrTi_{1-x}(Al_{0.5}Nb_{0.5})_xO_3$ ($0 \le x \le 0.15$) ceramics is investigated towards electric fields at room temperature in Fig. 4 (b). The magnitude of leakage current shows a strong dopant relationship with specified range of electric fields. When x = 0.03, the leakage current is larger than that of pure $SrTiO_3$ because of the more carriers introduced by doping. Although Al^{3+} and Nb^{5+} ions achieve the charge balance of +4 at Ti–site, the segregation of Al^{3+} and Nb^{5+} causes local charge imbalance which generates excess oxygen vacancies or electrons, both of which become mobile charge carriers and thus increase the conductivity loss. The leakage current decreases significantly at $0.05 \leq x \leq 0.10$. As shown in the SEM images, when x = 0.1, the grain size of the compound is nearly 6 times smaller than that of pure $SrTiO_3$, which leads to a huge increase in grain boundary amount. The chemical potential of grain boundary deviates from the integral value due to the lack of periodicity, resulting in the depletion layer formation at both sides of the grain boundary.[26–28] The depletion layer leads to the boundary bending of grain surface, and the potential barriers are formed on both sides of the grain boundary. The potential barriers would suppress carrier mobility thus reducing the conductivity loss.[29–31] As a result, the decreased grain size would devote to the reduction in leakage current. There is no obvious change in leakage current when x = 0.1 because of the excessive carriers introduced by increasing doping content. The growth of Qf values when x value increases from 0.05 to 0.10 indicates that the grain boundary limited conduction mentioned above limits the conductivity loss effectively when the grains become smaller. The great increase of leakage current at x = 0.15 could be attributed to the emergence of pores which is shown clearly in the SEM images. The appearance of porosity would result in a significant increase in leakage current. Similar phenomena have also been observed in other studies.[32–34] The Qf values decrease when x = 0.15

because of the markedly increased pores which resulting in simultaneous increase of defects and carriers.

4 SUMMARY

Al/Nb co–doped $SrTiO_3$ microwave ceramics with the composition of $SrTi_{1-x}(Al_{0.5}Nb_{0.5})_xO_3$ (x = 0.03, 0.05, 0.1 and 0.15) have been synthesized via a standard solid–state reaction method. The X–ray diffraction shows that perovskite structure compounds are prepared for all the compositions. The substitution of $(Al_{0.5}Nb_{0.5})^{4+}$ for Ti^{4+} induces a significant change in crystal structure and microscopic morphology, which brings a great influence on microwave dielectric properties. The isovalent doping introduces more mobile charge carriers and forms potential barriers on both sides of grain boundary. The potential barriers inhibit the transportation of carriers thus reducing the leakage current and resulting in the reduction of conductivity loss. The optimum microwave dielectric properties are ε_r ~185, Qf ~9077 GHz at 2.9 GHz for the $SrTi_{0.5}(Al_{0.5}Nb_{0.5})_{0.5}O_3$ ceramics.

ACKNOWLEDGMENT

This work was supported by the National Key Research and Development Program of China (Grant No. 2017YFB0406300), National Natural Science Foundation of China (Grant No. 61671326, 61701338) and Independent Innovation Fund of Tianjin University (No. 1705).

REFERENCES

1. Guo J, Baker AL, Guo HZ, Lanagan M, Randall CA. Cold sintering process: A new era for ceramic packaging and microwave device development. *J Am Ceram Soc*. 2017;100:669–677.

2. Song MZ, Iorsh I, Kapitanova P, Nenasheva E, Belov P. Wireless power transfer based on magnetic quadrupole coupling in dielectric resonators. *Appl Phys Lett*. 2016;108:023902.

3. Chang J, Liu ZF, Ma MS, Li YX. Parallel preparation and properties investigation on Li_2O–Nb_2O_5–TiO_2 microwave dielectric ceramics. *J Eur Ceram Soc*. 2017;37:3951–3957.

4. Zhou D, Guo D, Li WB, Pang LX, Yao X, Wang DW, Reaney IM. Novel temperature stable high–ε_r microwave dielectrics in the Bi_2O_3–TiO_2–V_2O_5 system. *J Mater Chem C*. 2016;4:5357–5362.

5. Gu FF, Chen GH, Yuan CL, Zhou CR, Yang Y. Low sintering temperature high permittivity ceramic composites for dielectric loaded microwave antennas. *J Mater Sci–Mater El*. 2015;26:360–368.

6. Qu JJ, Liu F, Wei X, Yuan CL, Liu XY, Chen GH, Feng Q. X–ray diffraction, dielectric, and raman spectroscopy studies of $SrTiO_3$–based microwave ceramics. *J Electron Mater.* 2016;45:715–721.

7. Liu F, Liu XY, Yuan CL, Yang T, Chen GH, Zhou CR. Crystal structure and dielectric properties of $(1-x)SrTiO_3$–$xCa_{0.4}Sm_{0.4}TiO_3$ ceramic system at microwave frequencies. *Mater Chem Phys.* 2014;148:1083–1088.

8. Zheng ZQ, Zhou XP. Reduction of Ti^{4+} to Ti^{3+} in boron doped $BaTiO_3$ at very low temperature. *J Am Ceram Soc*. 2013;96:3504–3510.

9. Negas T, Yeager G, Bell S, Coats N, Minis I. $BaTi_4O_9$/$Ba_2Ti_9O_{20}$–based ceramics resurrected for modern microwave applications. *Am Ceram Soc Bull.* 1993;72:80–89.

10. Qian XS, Ye HJ, Zhang YT, Gu H, Li X, Randall CA, Zhang QM. Giant electrocaloric response over a broad temperature range in modified $BaTiO_3$ ceramics. *Adv Funct Mater.* 2014;24:1300–1305.

11. Kuang XJ, Xia HT, Liao FH, Wang CH, Li L, Jing XP, Tang ZX. Doping effects of Ta on conductivity and microwave dielectric loss of $MgTiO_3$ ceramics. *J Am Ceram Soc*. 2007;90:3142–3147.

12. Zhang LY, Zhang J, Chang YF, Yuan GL, Yang B, Zhang ST. Composition dependent microstructures and properties of La , Zn , and Cr modified 0.675$BiFeO_3$–0.325$BaTiO_3$ ceramics. *J Am Ceram Soc*. 2016;99:2989–2994.

13. Fan XC, Chen XM, Liu XQ. Complex–permittivity measurement on high–Q materials via combined numerical approaches. *IEEE T Microw Theory*. 2005;53:3130–3134.

14. Goldschmidt VM. Die gesetze der krystallochemie. *Naturwissenschaften*. 1926;14:477–485.

15. Ratheesh R, Wöhlecke M, Berge B, Wahlbrink Th, Haeuseler H, Rühl E, Blachnik R, Balan P, Santha N, Sebastian MT. Raman study of the ordering in $Sr(B'_{0.5}Nb_{0.5})O_3$ compounds. *J Appl Phys*. 2000;88:2813–2818.

16. Glazer AM. The classification of tilted octahedra in perovskites. *Acta Crystallogr Sect B*. 1972;28:3384–3392.

17. Reaney IM, Colla EL, Setter N. Dielectric and structural characteristics of Ba– and Sr–based complex perovskites as a function of tolerance factor. *Jpn J Appl Phys*. 1994;33:3984.

18. Moreira RL, Lobo RPSM, Subodh G, Sebastian MT, Matinaga FM, Dias A. Optical phonon modes and dielectric behavior of $Sr_{1-3x/2}Ce_xTiO_3$ microwave ceramics. *Chem. Mater*. 2007;19:6548–6554.

19. Ullah B, Lei W, Cao QS, Zou ZY, Lan XK, Wang XH, Lu WZ. Structure and microwave dielectric behavior of A site doped $Sr_{(1-1.5x)}Ce_xTiO_3$ ceramics system. *J Am Ceram Soc*. 2016;99:3286–3292.

20. Kucheiko S, Choi JW, Kim HJ, Jung HJ. Microwave dielectric properties of $CaTiO_3$ $Ca(Al_{1/2}Ta_{1/2})O_3$ ceramics. *J Am Ceram Soc*. 1996;79:2739–2743.

21. Sebastian MT. Dielectric materials for wireless communication. *Elsevier*. 2010.

22. Shannon RD. Dielectric polarizabilities of ions in oxides and fluorides. *J Appl Phys*. 1993;73:348–366.

23. Zhang TW, Zuo RZ, Zhang J. Structure, microwave dielectric properties, and low temperature sintering of acceptor/donor codoped $Li_2Ti_{1-x}(Al_{0.5}Nb_{0.5})_xO_3$ ceramics. *J Am Ceram Soc*. 2016;99:825–832.

24. Kim SS, Park C. Leakage current behaviors of acceptor– and donor–doped $(Ba_{0.5}Sr_{0.5})TiO_3$ thin films. *Appl Phys Lett*. 1999;75:2554–2556.

25. Pullar RC, Penn SJ, Wang X, Reaney IM, Alford NM. Dielectric loss caused by oxygen vacancies in titania ceramics. *J Eur Ceram Soc*. 2009;29:419-424.

26. Meca F, Jonscher AK. Dielectric studies on sintered tantalum electrolytic capacitors. *Thin Solid Films*. 1979;59:201–219.

27. Gupta TK, Carlson WG. A grain–boundary defect model for instability/stability of a ZnO varistor. *J Mater Sci*. 1985;20:3487–3500.

28. Hower PL, Gupta TK. A barrier model for ZnO varistors. *J Appl Phys*. 1979;50:4847–4855.

29. Waser R, Klee M. Theory of conduction and breakdown in perovskite thin films. *Integr Ferroelectr*. 1992;2:23–40.

30. Krupanidhi SB, Peng CJ. Studies on structural and electrical properties of barium strontium titanate thin films developed by metallo–organic decomposition. *Thin Solid Films*. 1997;305:144–156.

31. Yang JK, Kim WS, Park HH. Effect of grain size of $Pb(Zr_{0.4}Ti_{0.6})O_3$ sol–gel derived thin films on the ferroelectric properties. *Appl Surf Sci*. 2001;169:544–548.

32. Weaver PM, Cain MG, Stewart M, Anson A, Franks J, Lipscomb IP, McBride JW, Zheng D, Swingler J. The effects of porosity, electrode and barrier materials on the conductivity of piezoelectric ceramics in high humidity and dc electric field. *Smart Mater Struct*. 2012;21:045012.

33. Singh R, Kulkarni AR, Harendranath CS. Effect of sintering temperature on composition, microstructure and electrical properties of $K_{0.5}Na_{0.5}NbO_3$ ceramics. *Physica B*. 2014;434:139–144.

34. Xie ZK, Peng B, Zhang J, Zhang XH, Yue ZX, Li LT. Effects of thermal anneal temperature on electrical properties and energy–storage density of $Bi(Ni_{1/2}Ti_{1/2})O_3$–$PbTiO_3$ thin films. *Ceram Int*. 2015;41:S206–S212.

Figure captions

Fig. 1. XRD patterns of $SrTi_{1-x}(Al_{0.5}Nb_{0.5})_xO_3$ ($0 \leq x \leq 0.15$) microwave ceramics.

Fig. 2. FE–SEM image of $SrTi_{1-x}(Al_{0.5}Nb_{0.5})_xO_3$ ($0 \leq x \leq 0.15$) microwave ceramics (a, plan view x=0; b, plan view, x=0.05; c, plan view, x=0.1; d, plan view, x=0.15).

Fig. 3. The dielectric constant and dielectric polarizability of $SrTi_{1-x}(Al_{0.5}Nb_{0.5})_xO_3$ ($0 \leq x \leq 0.15$) ceramics.

Fig. 4. (a) Qf and τ_f values of $SrTi_{1-x}(Al_{0.5}Nb_{0.5})_xO_3$ ($0 \leq x \leq 0.15$) ceramics; (b)leakage current of $SrTi_{1-x}(Al_{0.5}Nb_{0.5})_xO_3$ ($0 \leq x \leq 0.15$) ceramics towards electric fields.

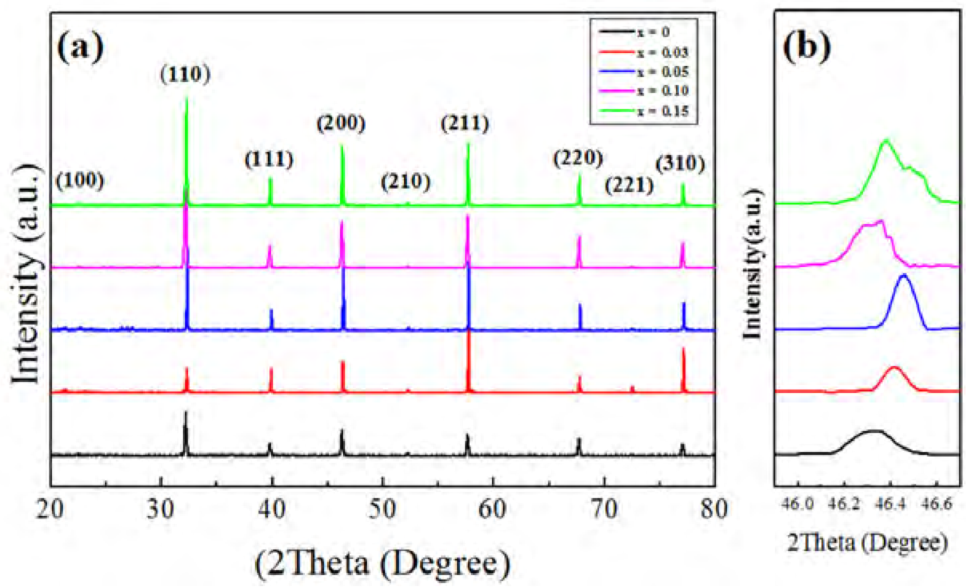
(a)
(b)
(100)
(110)
(111)
(200)
(210)
(211)
(220)
(221)
(310)
x = 0
x = 0.03
x = 0.05
x = 0.10
x = 0.15
Intensity (a.u.)
(2Theta (Degree)
Intensity(a.u.)
2Theta (Degree)
20
30
40
50
60
70
80
46.0
46.2
46.4
46.6

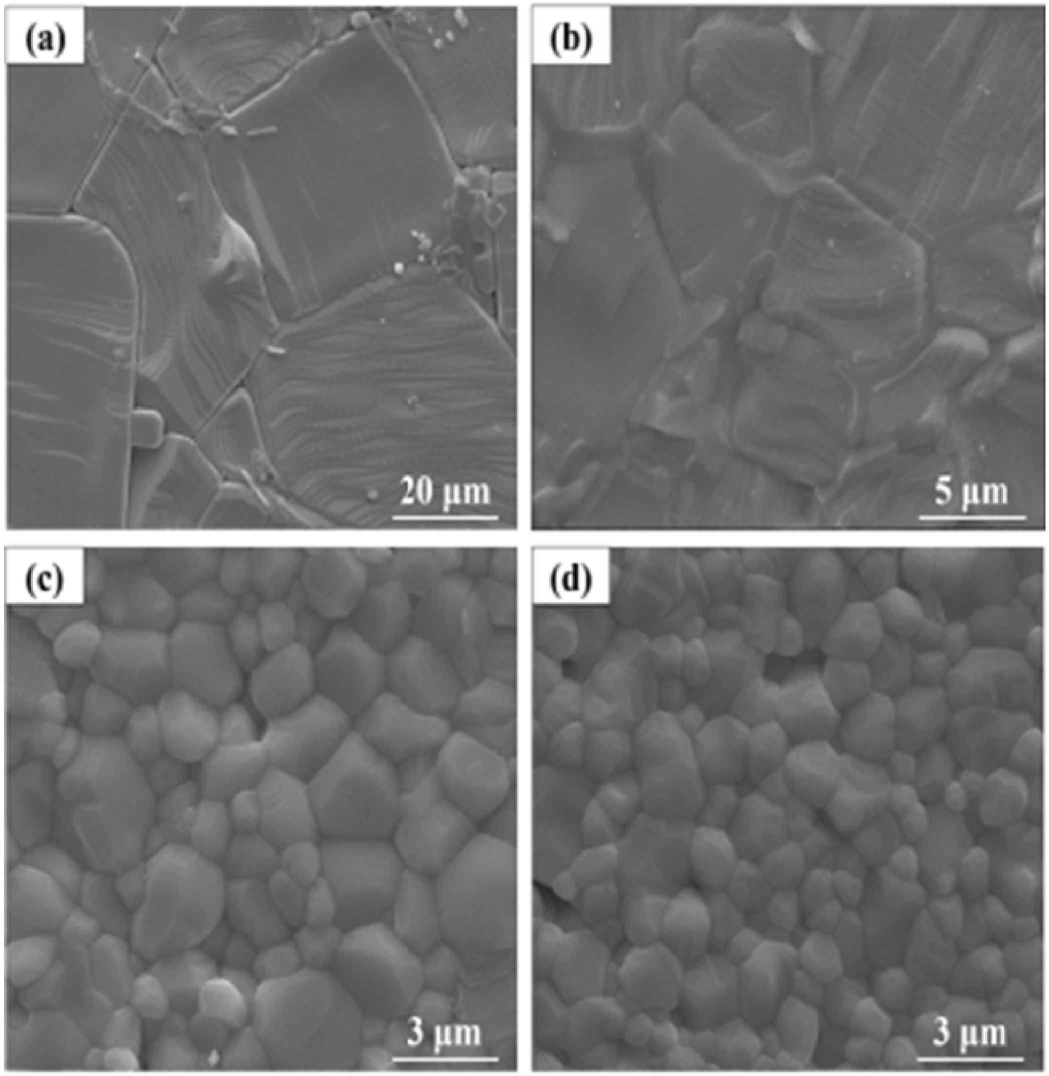
(a)
20 µm
(b)
5 µm
(c)
3 µm
(d)
3 µm

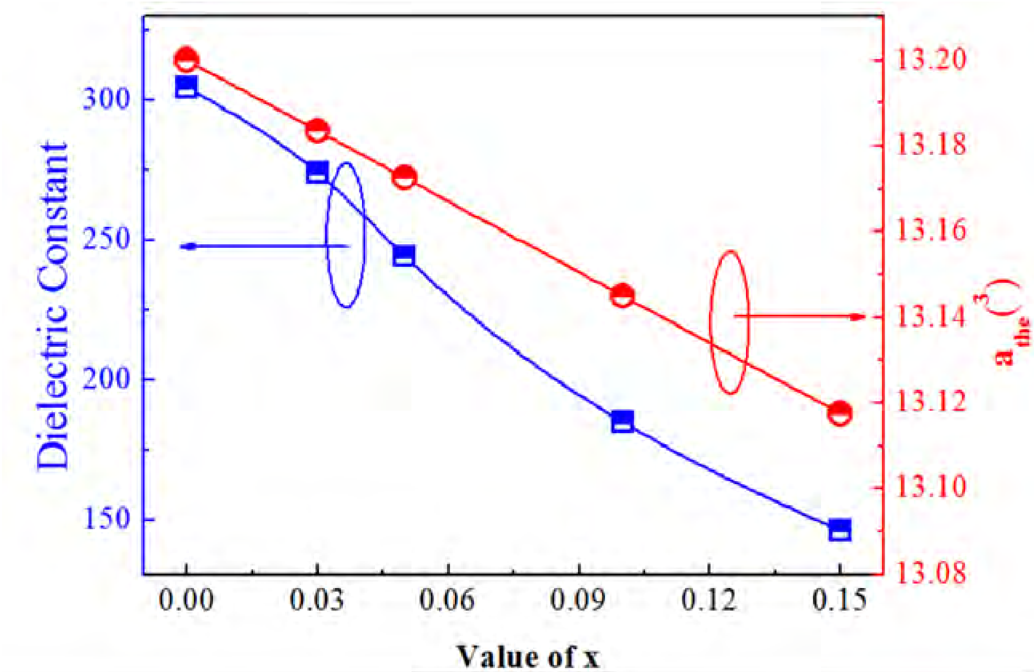

Dielectric Constant
300
250
200
150
13.20
13.18
13.16
13.14
13.12
13.10
13.08
a_the^3 ( )
0.00
0.03
0.06
0.09
0.12
0.15
Value of x

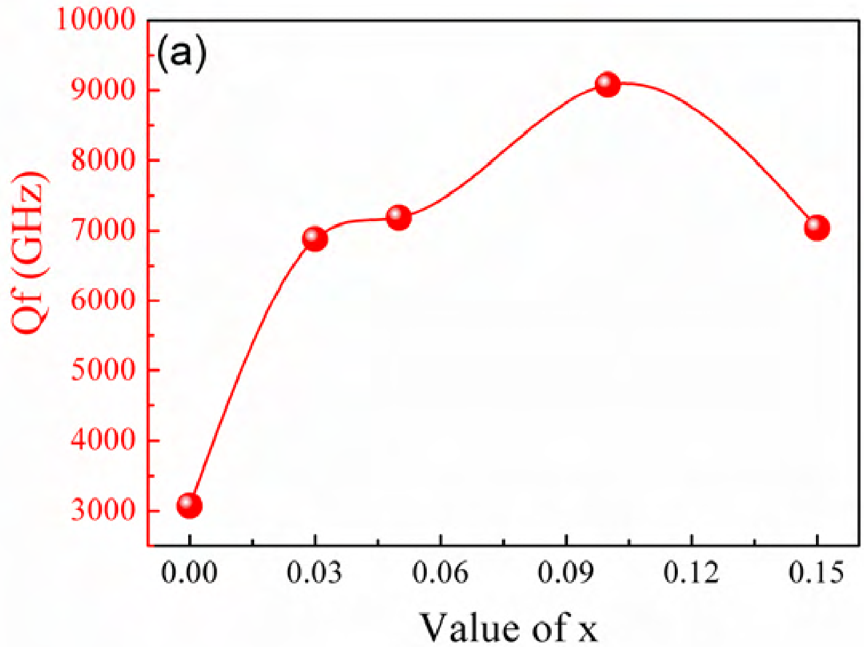
(a)
Qf (GHz)
10000
9000
8000
7000
6000
5000
4000
3000
0.00
0.03
0.06
0.09
0.12
0.15
Value of x

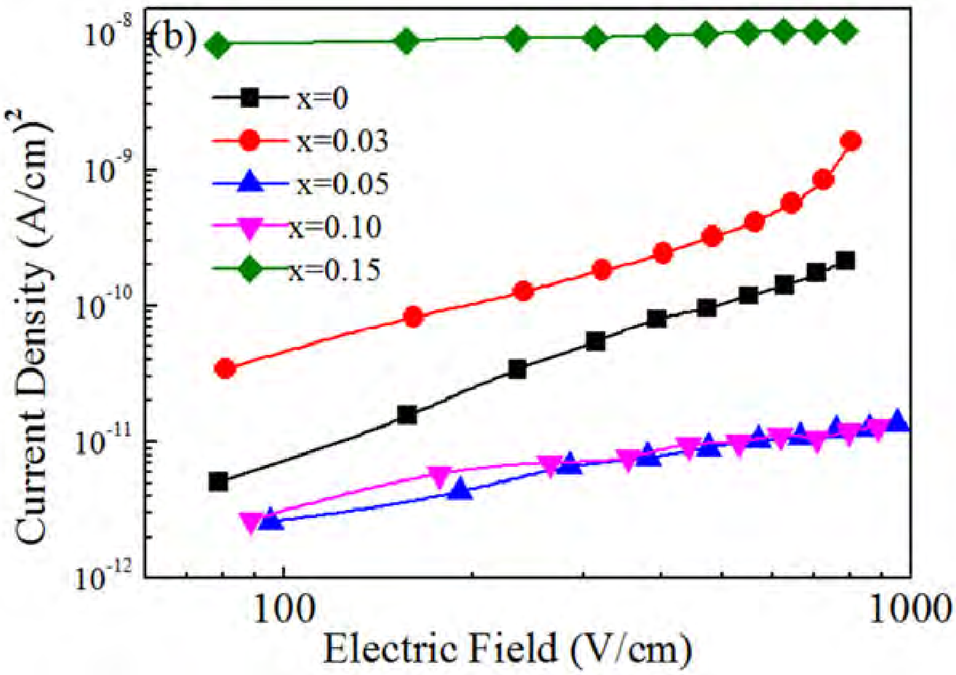
(b)
x=0
x=0.03
x=0.05
x=0.10
x=0.15
Current Density (A/cm)^2
10^{-8}
10^{-9}
10^{-10}
10^{-11}
10^{-12}
100
1000
Electric Field (V/cm)